

Effects of edge hydrogenation and Si doping on spin-dependent electronic transport properties of armchair boron-phosphorous nanoribbons

Hong Zhao(赵虹), Dan-Dan Peng(彭丹丹), Jun He(何军), Xin-Mei Li(李新梅), Meng-Qiu Long(龙孟秋)

Citation: Chin. Phys. B . 2018, 27(10): 108504. **doi:** 10.1088/1674-1056/27/10/108504

Journal homepage: http://cpb.iphy.ac.cn; http://iopscience.iop.org/cpb

What follows is a list of articles you may be interested in

Phase transition and charge transport through a triple dot device beyond the Kondo regime

Yong-Chen Xiong(熊永臣), Zhan-Wu Zhu(朱占武), Ze-Dong He(贺泽东)
Chin. Phys. B . 2018, 27(10): 108503. **doi:** 10.1088/1674-1056/27/10/108503

A phenomenological memristor model for synaptic memory and learning behaviors

Nan Shao(邵楠), Sheng-Bing Zhang(张盛兵), Shu-Yuan Shao(邵舒渊)
Chin. Phys. B . 2017, 26(11): 118501. **doi:** 10.1088/1674-1056/26/11/118501

An improved memristor model for brain-inspired computing

Errui Zhou(周二瑞), Liang Fang(方粮), Rulin Liu(刘汝霖), Zhenseng Tang(汤振森)
Chin. Phys. B . 2017, 26(11): 118502. **doi:** 10.1088/1674-1056/26/11/118502

Gas-sensor property of single-molecule device: F_2 adsorbing effect

Zong-Liang Li(李宗良), Jun-Jie Bi(毕俊杰), Ran Liu(刘然), Xiao-Hua Yi(衣晓华), Huan-Yan Fu(傅焕俨), Feng Sun(孙峰), Ming-Zhi Wei(魏明志), Chuan-Kui Wang(王传奎)
Chin. Phys. B . 2017, 26(9): 098508. **doi:** 10.1088/1674-1056/26/9/098508

Low-bias negative differential conductance controlled by electrode separation

Xiao-Hua Yi(衣晓华), Ran Liu(刘然), Jun-Jie Bi(毕俊杰), Yang Jiao(焦扬), Chuan-Kui Wang(王传奎), Zong-Liang Li(李宗良)
Chin. Phys. B . 2016, 25(12): 128503. **doi:** 10.1088/1674-1056/25/12/128503

Effects of edge hydrogenation and Si doping on spin-dependent electronic transport properties of armchair boron–phosphorous nanoribbons*

Hong Zhao(赵虹)[1], Dan-Dan Peng(彭丹丹)[1], Jun He(何军)[1,†], Xin-Mei Li(李新梅)[1], and Meng-Qiu Long(龙孟秋)[1,2,‡]

[1] *Hunan Key Laboratory of Super Micro-structure and Ultrafast Process, School of Physics and Electronics, Central South University, Changsha* 410083, *China*
[2] *Institute of Low-dimensional Quantum Materials and Devices, School of Physical Science and Technology, Xinjiang University, Urumqi* 830046, *China*

(Received 1 July 2018; revised manuscript received 24 July 2018; published online 10 September 2018)

In this article, the spin-dependent electronic and transport properties of the armchair boron–phosphorous nanoribbons (ABPNRs) are mainly studied by using the non-equilibrium Green function method combined with the spin-polarized density function theory. Our calculated electronic structures indicate that the edge hydrogenated ABPNRs exhibit a ferromagnetic bipolar magnetic semiconductor property, and that the Si atom doping can make ABPNRs convert into up-spin dominated half metal. The spin-resolved transport property results show that the doped devices can realize 100% spin-filtering function, and that the interesting negative differential resistance phenomenon can be observed. Our calculations suggest that the ABPNRs can be constructed as a spin heterojunction by introducing Si doping partially, and it would be used as a spin-diode for nano-spintronics in future.

Keywords: armchair boron–phosphorous nanoribbon, Si doping, bipolar magnetic semiconductor property, negative differential resistance

PACS: 85.35.–p, 73.63.–b, 75.75.–c, 72.15.Nj **DOI:** 10.1088/1674-1056/27/10/108504

1. Introduction

Owing to the unique structure and physical properties, two-dimensional (2D) materials have potential applications in electronics and spintronics devices and have attracted widespread attention in recent years.[1–9] Some interesting phenomena have been found in 2D materials, such as, spin-filtering,[10,11] the rectification effect,[12,13] negative differential resistance (NDR),[14–16] etc.

Seeking novel 2D candidate materials with high carrier mobility, mechanical stability, and high thermal stability, a moderate band gap has become crucial to a perfect electronic device. Recently, the III–V group semiconductors (B, P, As, Sb) 2D structures have received a great deal of attention,[17–25] of which the most prominent is boron phosphide (BP). Theoretical researches show that the single layer hexagonal boron phosphide (h-BP) is a direct-gap semiconductor[26] and has high electron mobility and hole mobility.[27–29] Experiments show that BP has good stability.[18,20] Overall h-BP would be a candidate for future optical and electronic devices.

Up to now, only a few attempts have been made to understand the mechanical electronic properties in pristine h-BP, but whether the spin-dependent electronic transport properties of the h-BP can be modulated is still unknown to us. Generally, edge modifications or doping atoms can affect the magnetic and electrical properties in unexpected ways, which are commonly used to modulate artificially the electronic structures and spin transport properties of 2D materials based nanodevices, such as graphene,[30–33] graphdiyne,[34,35] silicene,[36,37] phosphorene,[38] etc. Recent studies have revealed that when the B or P atom in h-BP is passivated with hydrogen, the h-BP becomes a metal which exhibits a giant spin splitting effect, and the spin density distribution is independent of the atom bonded with H, but localized on the other two adjacent atoms.[39] In addition, monolayer semiconductors can also be functionalized by doping which can significantly change the electronic properties. The doping atoms can change the local atomic configuration of the host system and their electronic structures are substantially modified.[40,41] However, so far how the edge modifications and doping atoms affect the electronic transport properties of h-BP is unclear. Owing to the previous work showing that the zigzag boron–phosphorous nanoribbons (ZBPNRs) are metallic while the armchair boron–phosphorous nanoribbons (ABPNRs) are semiconductor,[17] in this paper we study the effects of the edge hydrogenation and silicon (Si) doping on the elec-

*Project supported by the National Natural Science Foundation of China (Grant No. 21673296), the Hunan Provincial Natural Science Foundation of China (Grant No. 2018JJ2481), and the Fundamental Research Funds for the Central Universities of Central South University, China (Grant No. 2018zzts328).

†Corresponding author. E-mail: junhe@csu.edu.cn
‡Corresponding author. E-mail: mqlong@csu.edu.cn

© 2018 Chinese Physical Society and IOP Publishing Ltd

tronic and spin-dependent transport properties of the ABPNRs.

2. Models and methods

The first-principles calculation software used in this paper is the Atomistix ToolKit (ATK) package,[42] which is based on the spin-polarized density functional theory (DFT)[43] and the non-equilibrium Green's function (NEGF). The exchange–correlation functional selects and uses the generalized gradient approximation.[44] The k-points selected in the x, y, and z directions are 1, 1, 100, where the z direction represents the direction of electron transport. In order to avoid the interaction between layers, the vacuum layer of 15 Å is selected. The cutoff energy is 150 Ry (1 Ry = 13.6056923 eV). When the structure is optimized, the convergence standard of the system is set to be 0.01 eV/Å, and the total energy is converged to 10^{-5} eV. Applying the double-zeta polarized basis to wave functions, the electrode temperature is 300 K. Open boundary conditions are used to describe the electronic and transport properties of the nano-devices. The spin-polarized current through the system is calculated by using the Landauer–Buttiker formula[45]

$$I_\sigma(V_\mathrm{b}) = \frac{e}{h}\int_{\mu_\mathrm{L}(V_\mathrm{b})}^{\mu_\mathrm{R}(V_\mathrm{b})} \{T_\sigma(E,V_\mathrm{b}) \times [f_\mathrm{L}(E,V_\mathrm{b}) - f_\mathrm{R}(E,V_\mathrm{b})]\}\,\mathrm{d}E. \quad (1)$$

Here, e is the electron charge, h is Planck's constant, T_σ is the transmission, and σ refers to the spin state. $f_{\mathrm{L(R)}}(E,V_\mathrm{b})$ is the Fermi–Dirac distribution function of the left (right) electrode, which depends on the external bias voltage V_b. Here in this work, T_σ is obtained from the following equation:

$$T_\sigma(E,V_\mathrm{b}) = \mathrm{Tr}\left[\mathrm{Im}\left\{\Sigma^\mathrm{r}_{\mathrm{L}_\sigma}(E,V_\mathrm{b})\right\} G^\mathrm{r}_\sigma(E,V_\mathrm{b}) \times \mathrm{Im}\left\{\Sigma^\mathrm{r}_{R_\sigma}(E,V_\mathrm{b})\right\} G^\mathrm{a}_\sigma(E,V_\mathrm{b})\right]. \quad (2)$$

Here, $G^\mathrm{r}_\sigma\,(G^\mathrm{a}_\sigma)$ is the retarded (advanced) Green function matrix, and $\Sigma^\mathrm{r}_{\mathrm{L}_\sigma}\left(\Sigma^\mathrm{r}_{R_\sigma}\right)$ is the retarded self-energy matrix for the left (right) electrode.

According to the number of boron (B) atoms on the ABPNRs, the studied system can be denoted as N-ABPNR, and Fig. 1(a) shows the model of 7-ABPNR. Note that the edges of ABPNRs are saturated with hydrogen (H) atoms to improve the stability of the system. Each of the edge B atoms is saturated by one H atom, and the edge P atom is saturated by two H atoms.

3. Results and discussion

Firstly, we calculate the formation energy of 7-ABPNR, which is based on the formula $E_\mathrm{form} = E^\mathrm{tol}_{7-\mathrm{ABPNR}} - \left(E^\mathrm{tol}_\mathrm{ABPNR} + \frac{1}{2}N_\mathrm{H}E_{\mathrm{H}_2}\right)$, where $E^\mathrm{tol}_{7-\mathrm{ABPNR}}$, $E^\mathrm{tol}_\mathrm{ABPNR}$, N_H, and E_{H_2} represent the total energy of the 7-ABPNR, the total energy of the 7-ABPNR without modifying by H atoms, the number of H atoms, and the energy of the isolated H_2 molecules, respectively. The calculated formation energy for 7-ABPNR is -6.22 eV, indicating that the edge hydrogenation improves the stability of 7-ABPNR. Moreover, we calculate the energies in the three spin states of ferromagnetic (FM), antiferromagnetic (AFM), and nonmagnetic (NM), respectively. Taking 7-ABPNR for example, our results show that the total energy of 7-ABPNR in NM is 2.75 meV higher than that in AFM, and it is 64.32 meV higher than that in FM. Thus, we can infer that the FM magnetic configuration would be the ground state for ABPNRs.

As shown in Figs. 1(b)–1(d), we calculate the energy band structures of 6-ABPNR, 7-ABPNR, and 8-ABPNR unit cells, denoted as M0, M1, and M2, respectively. It is interesting that the spin-splitting behavior can be observed clearly for each ABPNR, in which there are two down-spin subbands that are above the fermi level (FL), and two up-spin subbands that are below the FL. This phenomenon shows that the N-ABPNR is a bipolar magnetic semiconductor (BMS). The distinctiveness of BMS lies in the fact that the valence band (VB) and conduction band (CB) approaching to the FL have opposite spin channels, which can provide completely spin-polarized currents with tunable spin polarization by regulating the FL.[46] Such a spin-splitting behavior of ABPNRs would open a new way to spintronic devices.

To further illustrate the nature of electronic structure, the density of state (DOS), projected density of state (PDOS), and spin density distribution of 7-ABPNR are calculated, which can be seen in Fig. 1(e). We can see from the 7-ABPNR DOS that there are two spin-splitting peaks near the FL, the spin-down peak is above the FL, and the spin-up peak is below the FL, which corresponds to the energy band structure. From the PDOS, we can find that the spin-spilt DOS peaks are mainly caused by the p orbits of the B atoms.

In the following, taking 7-ABPNR for example, the two-probe device structure used in transport calculations is shown in Fig. 2(a). This device is denoted as M3 and is divided into three areas, namely the left electrode, the right electrode, and the scattering area. Here, the electrode with 7-ABPNR in the ground state is modeled as being semi-infinite. Owing to the fact that the FM state for ABPNRs could be realized by using a certain magnetic or electronic field, we describe two spin configurations, in which the spin orientations between two electrodes are parallel configuration (PC) and antiparallel configuration (APC), corresponding to [1, 1] and [1, −1] magnetic configurations, respectively.

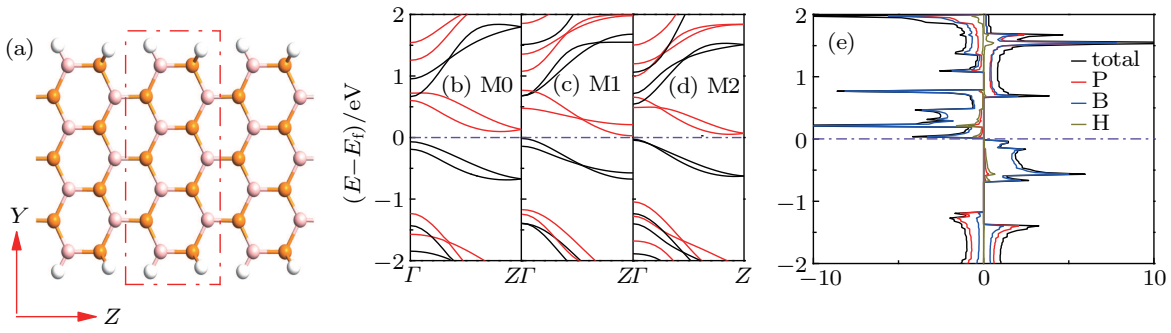


Fig. 1. (color online) (a) Structure of 7-ABPNR along z aixs, the red dashed rectangle represents the unit cell. (b)–(d) Band structures of 6-ABPNR, 7-ABPNR, and 8-ABPNR, the black and red lines refer to up-spin and down-spin states, respectively. (e) DOS and PDOS of 7-ABPNR in FM state. Pink, orange, and white balls denote B, P, and H atoms, respectively.

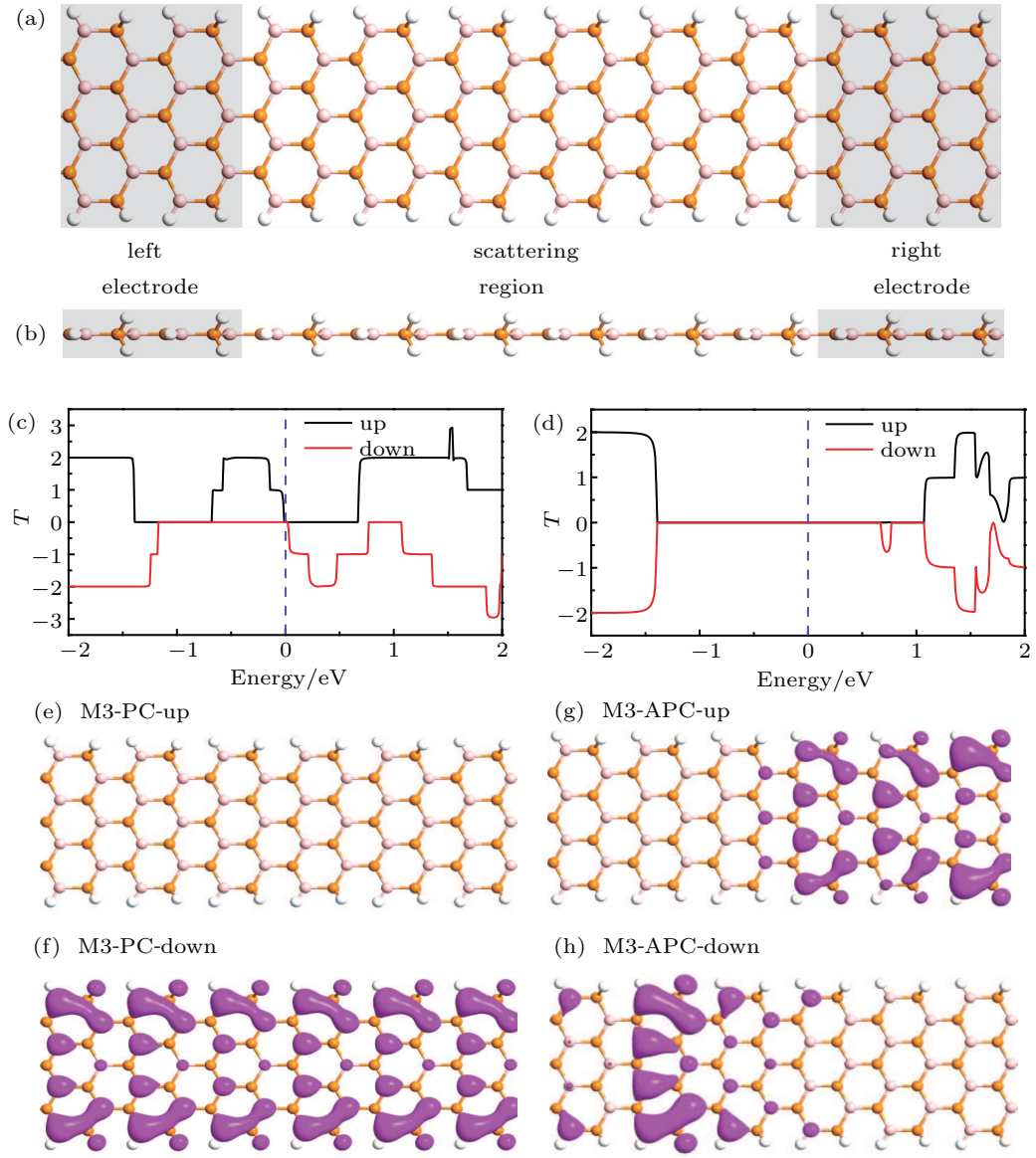


Fig. 2. (color online) (a) Top view and (b) side view of the two-probe system of M3. (c) [(d)] TS for M3 in PC [APC] at 0.0 V. (e)–(h) refer to LDOS of M3 in 0.3 eV at 0.0 V, followed by up-spin state in PC, down-spin state in PC, up-spin state in APC, and down-spin state in APC, respectively, and the isovalue is 0.1 Å^{-3}.

The transmission spectrum (TS) of M3 at 0.0 V in PC is shown in Fig. 2(c). It can be observed that the positive and negative energy regions near the FL are occupied by the two opposite spin bands, which means a fully bipolar spin filtering effect. Then, as plotted in Figs. 2(e)–2(f), to further explain the spin polarization of TS, the local density of state (LDOS)

of M3 at 0.3 eV is given. It can be observed that there is no up-spin electron density, and the up-spin electrons cannot be transmitted in the device either. For the down-spin state, it can be found that the electron density is delocalized throughout the device and the down-spin electrons can pass through the transmission channel from the left electrode to the right electrode. Moreover, the TS for M3 in APC at 0.0 V is also shown in Fig. 2(d). The transmission spectra for both spin states are zero near the FL, and we can find that the LDOS of M3 at 0.3 eV in APC is localized for each spin state, and the corresponding electrons passing through channels are suppressed.

Next, we also consider the electronic structure and spin-dependent transport on the Si doped 7-ABPNR. Also, the calculation of the energy difference among Si doped 7-ABPNRs with different spin states indicates that the ferromagnetic state has the lowest energy, therefore we built a two-probe system (marked as M4) as shown in Fig. 3(a), and the corresponding electronic transport properties are calculated. The transmission spectra of M4 in PC and APC at bias of 0.0 V are plotted in Figs. 3(b)–3(c), respectively. We can clearly see that the TS in PC is spin-splitting, while that in APC is degenerate. Comparing with the TS of M3 at 0.0 V in PC, it can be found that the doping of Si atoms results in the up-spin TS moving to the positive energy region and across the FL, and thus M4 with FM spin configuration present the perfect spin-filtering and half-metallic property around the FL. Moreover, figures 3(d)–3(e) show the LDOS of M4 in PC, where the distribution of the up-spin state is delocalized, which is in favor of the electron transmission. Nevertheless, one cannot find any electronic density for the down-spin state in Fig. 3(e), which indicates that the corresponding transport channel is forbidden. Also, the up-spin and down-spin LDOS of M4 in APC at 0.0 V are shown in Figs. 3(f)–3(g), and we can see that the electron density is localized for each spin state, which is consistent with the result that no transmission coefficient appears near the FL in Fig. 3(c).

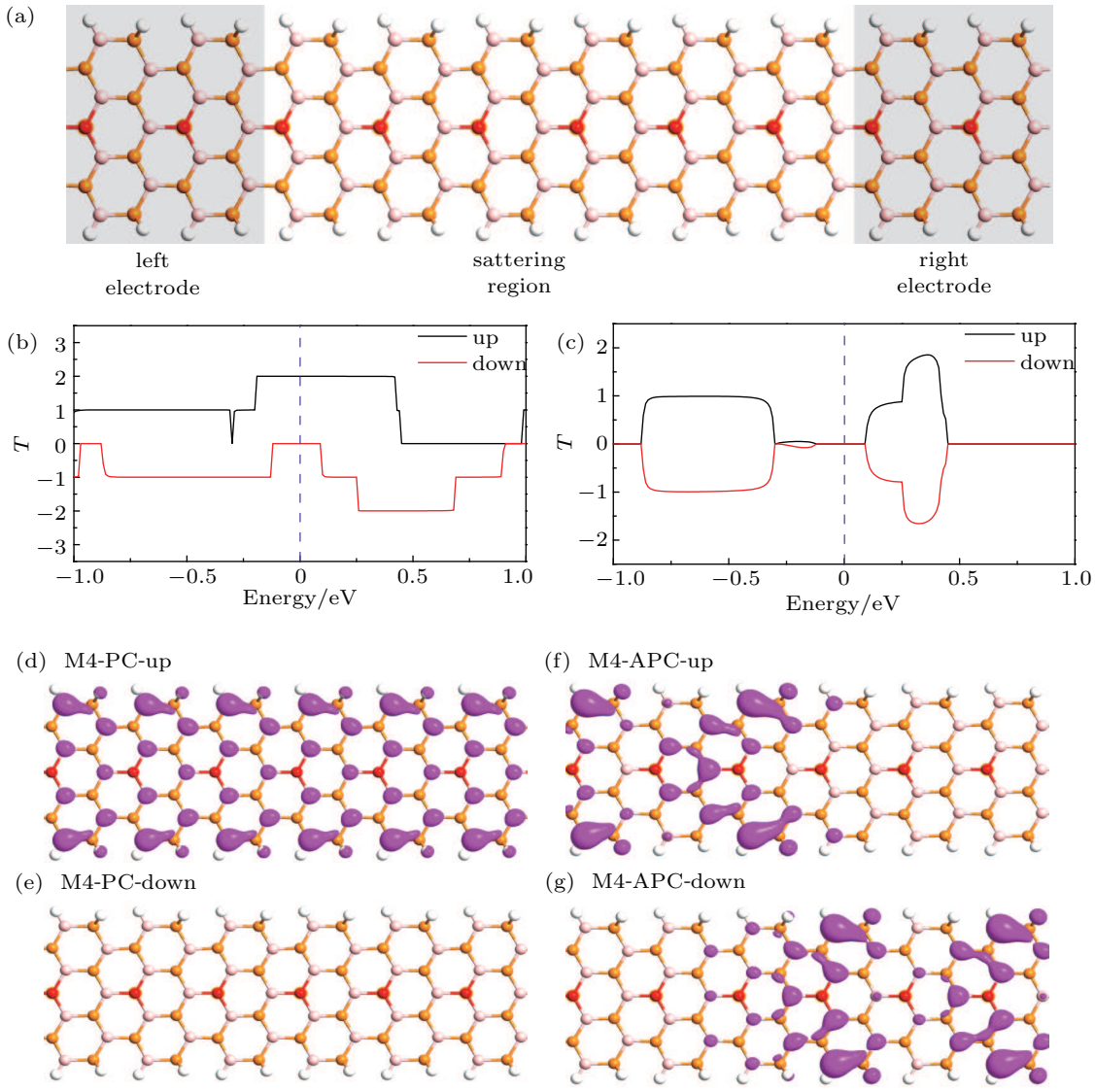


Fig. 3. (color online) (a) Two-probe system of M4. (b) [(c)] TS for M4 in PC [APC]. (d) [(e)], (f) [(g)] LDOS of up-spin [down-spin] for M4 in PC [APC] at the FL under bias of 0.0 V, the isovalue is 0.1 Å^{-3}. The Si atoms are denoted by a red ball.

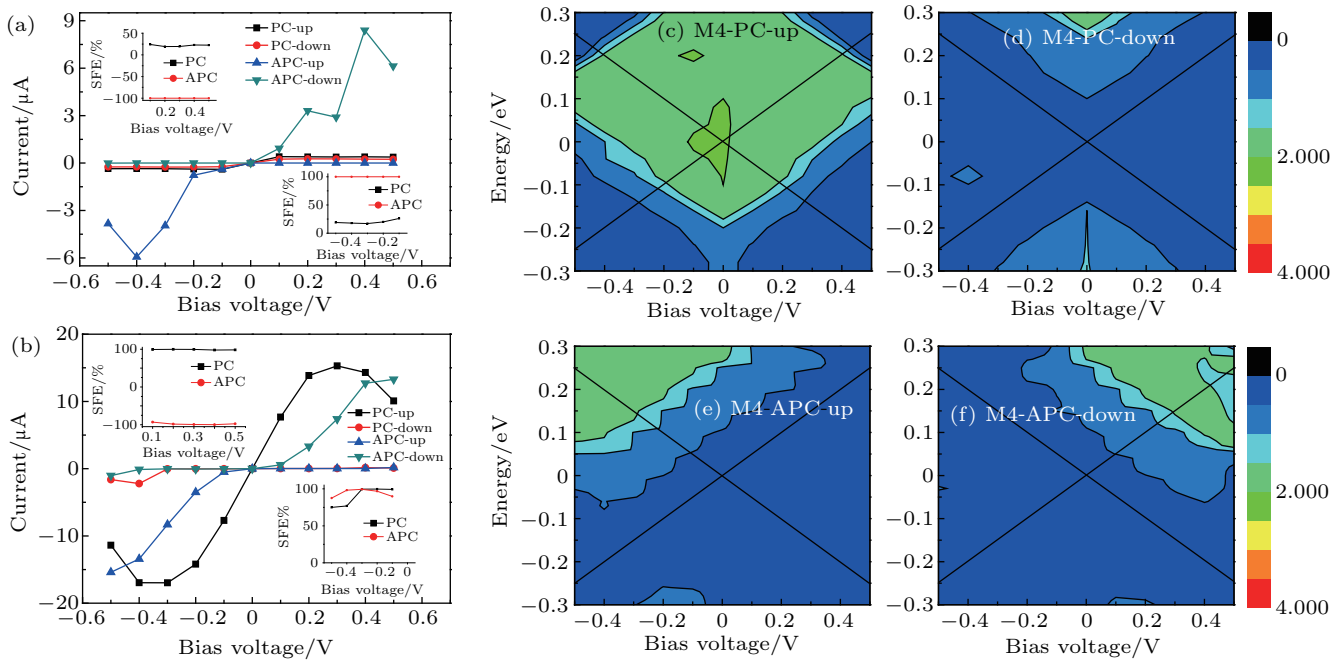


Fig. 4. (color online) (a) [(b)] I–V curves of M3 M4, with insets showing SFE. (c) and (d) [(e) and (f)] Spin-resolved TS as a function of electron energy and BV for M4 in PC [APC]. Region between black solid lines denotes BW, and negative (positive) BW is on the left (right).

In the following, we simulate the spin-dependent transport properties of the ABPNRs systems. By applying a bias voltage (BV) across the left electrode and the right electrode, the corresponding I–V curve of the device can be obtained. As shown in Fig. 4(a), we can find that the current of M3 in PC is almost zero throughout the bias voltage region ([−0.5 V, 0.5 V]). As for the APC spin configuration, there is only down-spin current in the positive bias region, and the negative bias region is opposite to it, indicating that M3 in APC has an ideal bipolar spin-filtering effect. Furthermore, in the bias region of [0 V, 0.5 V], the down-spin current increases first when BV $<$ 0.2 V, reaches a maximum at BV $=$ 0.4 V, and then starts to decrease, which indicates that the down-spin current has an NDR effect. The up-spin current in a bias region of [−0.5 V, 0 V] is symmetrical with respect to the down-spin current in the bias region of [0 V, 0.5 V], and an interesting NDR effect has also been observed.

When the Si atoms are introduced, the I–V curves are very different, which can be seen in Fig. 4(b). For M4 in PC, one can see that only the up-spin current appears in the entire bias voltage range, which indicates that the up-spin electrons pass through the transmission channel, and the down-spin electrons are suppressed. For a more intuitive view of spin filtering, we calculate the spin-filtering efficiency (SFE) from the formula SFE $= \left|\left(I_{\uparrow} - I_{\downarrow}\right) / \left(I_{\uparrow} + I_{\downarrow}\right)\right| \times 100\%$. As shown in Fig. 4(a), the SFE is greater than 99% in most of the bias range, which shows that M4 has excellent spin filtering characteristics. Moreover, in the bias region of [−0.5 V, 0 V], the up-spin current increases first when BV $<$ 0.3 V, reaches a maximum at BV $=$ 0.3 V, and then starts to decrease, which shows the NDR effect for the up-spin current of M4. In addition, for M4 in APC, it can be seen that the positive bias region has only down-spin current, and the reverse bias region is opposite, which indicates that M4 has a perfect bipolar spin-filtering effect.

We also give the spin-resolved TS as a function of electron energy and bias voltage for M4 with PC and APC spin configurations in Figs. 4(c)–4(f), respectively. The integral of the $T\left(E, V_{\mathrm{b}}\right)$ in the bias window (BW) determines the magnitude of the current as shown in Figs. 4(c) and 4(d), when the applied bias increases, the up-spin transmission peak enters into the BW while the down-spin transmission peak is absent, which leads to only the up-spin current conducting, and thus M4 shows a perfect spin-filtering effect. Also, we can see that the area of the up-spin TS in the BW first increases and then decreases, thus resulting in the NDR phenomenon of up-spin current of M4 in PC. Furthermore, as shown in Fig. 4(e), there are transmission peaks in the negative bias region rather than in the negative bias region for the up-spin state of M4 in APC, as a result, the up-spin current of M4 in the negative bias region is much larger than that in the positive region. The reverse can be observed for the down-spin state, namely, the down-spin current of M4 in the positive bias region is much larger than that in the negative region.

To gain an in-depth understanding of the mechanism of spin transport of Si doped ABPNR, figures 5(a) and 5(b) show the band structures and corresponding transmission spectra of the left and right electrode under PC and APC with a BV of 0.3 V. For M4 in PC, when the external BV is 0.3 V, the energy band of the left electrode part moves down by 0.15 eV

while the right electrode is opposite to it, which can be seen in Fig. 5(a). The left and right electrode have up-spin energy bands that enter into the BW and overlap each other inside, although both the left and right electrodes have down-spin energy bands that enter into the BW but have no overlapping portions. Therefore, the up-spin transmission peak in the BW has no down-spin transmission peak, and thus leading M4 to have a perfect spin-filtering behavior. For M4 in APC, which is shown in Fig. 5(b), the addition of a 0.3 V bias makes the bands of the left (right) electrode shift downward (upward) by 0.15 eV, the down-spin energy bands of the left and right electrode overlap each other within the BW, and only the right electrode has the up-spin band enter into the BW, so there is only the down-spin transmission peak in the BW.

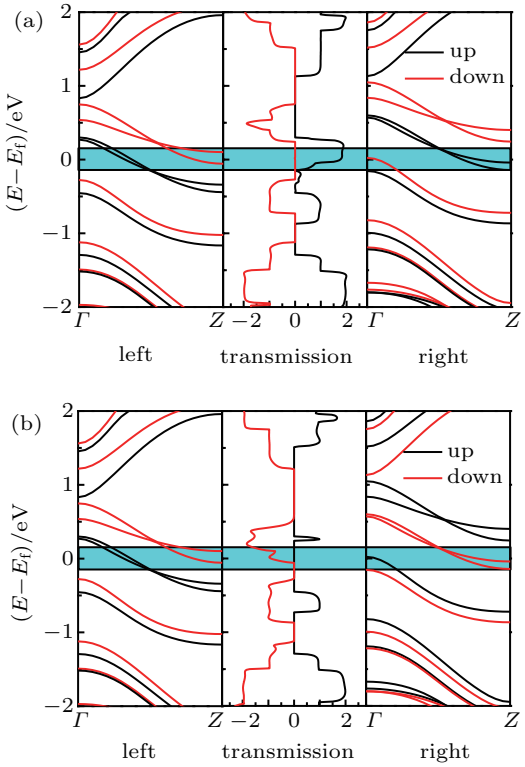


Fig. 5. (color online) (b) [(c)] Band structures for the left electrode (left panels), transmission (middle panels) and band structures for the right electrode (right panels) of M4 in PC [APC] at $V_b = 0.3$ V. The blue area refers to BW.

The above calculations show that the ABPNR is a ferromagnetic bipolar magnetic semiconductor, and when a P atom is replaced by an Si atom, the up-spin would cross the FL, and leads the system to exhibit the half-metallic property in the FM state. Then, we built a heterojunction (marked as M5), which is shown in Fig. 6(a), in which the left part is for the perfect 7-ABPNR and the right part is for the Si doped 7-ABPNR. The calculated *I*–*V* curves can be seen in Fig. 6(b). For M5 in the PC spin configuration, one can find that the down-spin current is almost zero in the entire bias region [−0.5 V, 0.5 V], while the up-spin current only appears in the negative bias region and linearly increases below 0.5 V. We can find that M5 acts as a perfect bipolar spin-filter in the APC spin configuration, showing that the down-spin current only appears in the positive bias region and the up-spin current only appears in the negative bias region. In order to be more intuitive, three-dimensional transmission spectra are shown in Figs. 6(c)–6(f). We can find that there are considerable spin-up transmission peaks in the negative bias region but hardly any value in the positive bias region, which is shown in Fig. 6(c), indicating that only the spin-up current of M5 in PC appears in the negative bias region. For the down-spin situation, there is no transmission peak appearing in the whole BW, so the corresponding current is zero, and thus a single polarized spin-filtering effect can be observed for M5 in the PC spin configuration. Furthermore, for M5 in APC, the spin-up current is the same as in the case of PC, while the down-spin current in the positive bias region is much larger than that in the negative region. As a result, the perfect bipolar spin-filtering effect can be observed for M5 in the APC spin configuration.

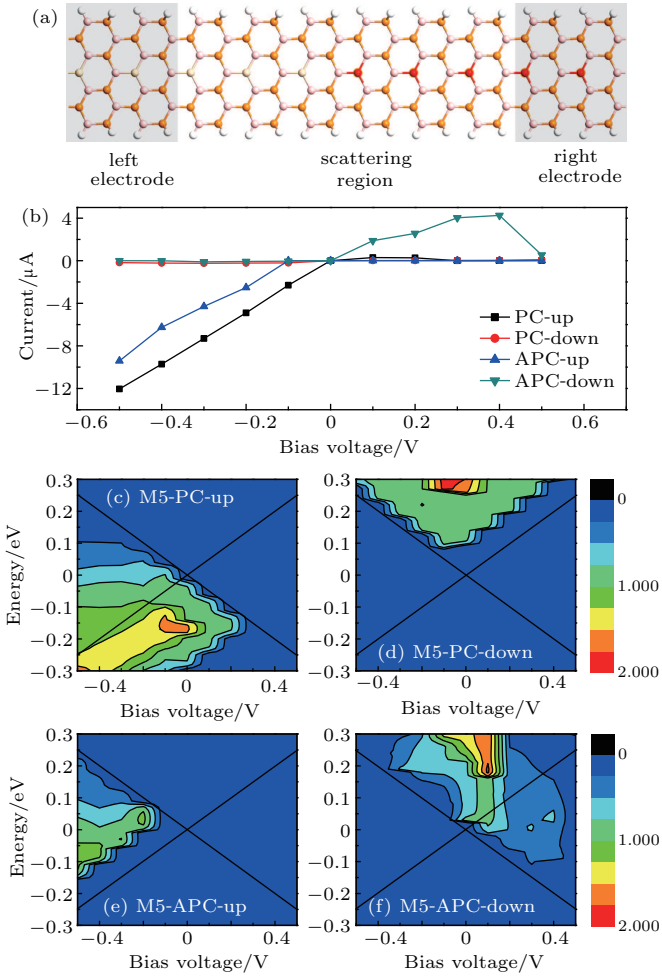


Fig. 6. (color online) (a) Two-probe system of M5. (b) *I*–*V* curve of M5. (c) and (d) [(e) and (f)] Spin-resolved transmission as a function of electron energy and BV for M5 in PC [APC].

4. Conclusions

In summary, the electronic structures and transport properties of the two systems of ABPNRs and Si-doped ABPNRs

have been studied. The results show that the ground state of ABPNRs is an FM configuration and exhibits the properties of BMS behavior, which is independent of ribbon width. The 7-ABPNR device has a bipolar spin-filtering phenomenon and an NDR phenomenon under APC spin configuration. The introduced Si atom doping can transform ABPNRs from BMS into up-spin dominated semi-metal, and the 100% spin filtering and obvious NDR phenomenon of the Si-doped ABPNR device can be observed. Moreover, we also build a heterojunction based on the pristine ABPNR and Si-doped ABPNR, and find that the single polarized spin-filtering effect can happen in the PC spin configuration, while the perfect bipolar spin-filtering effect happens in the APC spin configuration. Our results suggest the ABPNR would be a candidate material for applications in nanoelectronic and spintronics devices due to its attractive spin-dependent electronic transport properties.

References

[1] Geim A K and Novoselov K S 2007 *Nat. Mater.* **6** 183
[2] Jose D and Datta A 2011 *Phys. Chem. Chem. Phys.* **13** 7304
[3] Li L K, Yu Y J, Ye G J, Ge Q Q, Ou X D, Wu H, Feng D L, Chen X H and Zhang Y B 2014 *Nat. Nanotechnol.* **9** 372
[4] Liu H, Neal A T, Zhu Z, Luo Z, Xu X F, Tomanek D and Ye P D 2014 *ACS Nano* **8** 4033
[5] Long M Q, Tang L, Wang D, Li Y L and Shuai Z G 2011 *ACS Nano* **5** 2593
[6] Wang Q H, Kalantar-Zadeh K, Kis A, Coleman J N and Strano M S 2012 *Nat Nanotechnol.* **7** 699
[7] Xiao J, Long M Q, Zhang X J, Ouyang J, Xu H and Gao Y L 2015 *Sci. Rep.* **5** 09961
[8] Michetti P and Recher P 2011 *Phys. Rev. B* **84** 125438
[9] Bi J Y, Han L H, Wang Q, Wu L Y, Quhe R G and Lu P F 2018 *Chin. Phys. B* **27** 026802
[10] Deng X Q, Zhang Z H, Tang G P, Fan Z Q and Yang C H 2014 *Rsc Adv.* **4** 58941
[11] Zhao C C, Tan S H, Zhou Y H, Wang R J, Wang X J and Chen K Q 2017 *Carbon* **113** 170
[12] Nazirfakhr M and Shahhoseini A 2018 *Phys. Lett. A* **382** 704
[13] Zhou Y H, Lei Y and Peng Y L 2015 *Aer. Adv. Eng. Res.* **21** 267
[14] Jiang B, Zhou Y H, Chen C Y and Chen K Q 2015 *Org. Electron.* **23** 133
[15] Husain M M and Kumar M 2015 *Org. Electron.* **27** 92
[16] Chen L N, Ma S S, Ouyang F P, Wu X Z, Xiao J and Xu H 2010 *Chin. Phys. B* **19** 097301
[17] Zeng B W, Li M J, Zhang X J, Yi Y G, Fu L P and Long M Q 2016 *J. Phys. Chem. C* **120** 25037
[18] Sahin H, Cahangirov S, Topsakal M, Bekaroglu E, Akturk E, Senger R T and Ciraci S 2009 *Phys. Rev. B* **80** 155453
[19] Lopez-Castillo A 2012 *Int. J. Quantum Chem.* **112** 3152
[20] Wang S F and Wu X J 2015 *Chin. J. Chem. Phys.* **28** 588
[21] Wu M H, Zhang Z H and Zeng X C 2010 *Appl. Phys. Lett.* **97** 093109
[22] Sohbatzadeh Z, Roknabadi M R, Shahtahmasebi N and Behdani M 2015 *Physica E* **65** 61
[23] Wang Y L and Shi S Q 2010 *Solid State Commun.* **150** 1473
[24] Cakir D, Kecik D, Sahin H, Durgun E and Peeters F M 2015 *Phys. Chem. Chem. Phys.* **17** 13013
[25] Yang K W, Li M J, Zhang X J, Li X M, Gao Y L and Long M Q 2017 *Chin. Phys. B* **26** 098509
[26] Zhuang H L L and Hennig R G 2012 *Appl. Phys. Lett.* **101** 153109
[27] Peelaers H and Van de Walle C G 2012 *Phys. Rev. B* **86** 241401
[28] Dong Y L, Zeng B W, Xiao J, Zhang X J, Li D D, Li M J, He J and Long M Q 2018 *J. Phys.: Condens. Matter* **30** 125302
[29] Low T, Rodin A S, Carvalho A, Jiang Y J, Wang H, Xia F N and Neto A H C 2014 *Phys. Rev. B* **90** 075434
[30] Zhang D, Long M, Zhang X, Cui L, Li X and Xu H 2017 *J. Appl. Phys.* **121** 093903
[31] Zhang D, Long M, Zhang X, Ouyang F, Li M and Xu H 2015 *J. Appl. Phys.* **117** 014311
[32] Wang G, Long M Q and Zhang D 2017 *Chin. Phys. Lett.* **34** 097303
[33] Pan C N , Long M Q and He J 2018 *Chin. Phys. B* **27** 088101
[34] Li M, Zhang D, Gao Y, Cao C and Long M 2017 *Org. Electron.* **44** 168
[35] Li X B, Cao L M, Long M Q, Liu Z R and Zhou G H 2018 *Carbon* **131** 160
[36] Zhang X, Zhang D, Xie F, Zheng X, Wang H and Long M 2017 *Phys. Lett. A* **381** 2097
[37] Shirzadi B and Yarmohammadi M 2017 *Chin. Phys. B* **26** 017203
[38] Xie F, Fan Z Q , Zhang X J , Liu J P , Wang H Y , Liu K, Yu J H and Long M Q 2017 *Org. Electron.* **42** 21
[39] Yu J and Guo W 2015 *Appl. Phys. Lett.* **106** 043107
[40] Onat B, Hallioglu L, Ipek S and Durgun E 2017 *J. Phys. Chem. C* **121** 4583
[41] Özçelik V O, Kecik D, Durgun E and Ciraci S 2015 *J. Phys. Chem. C* **119** 845
[42] Taylor J, Guo H and Wang J 2001 *Phys. Rev. B* **63** 245407
[43] Baerends E J 2000 *Theor. Chem. Acc* **103** 265
[44] Boese A D, Doltsinis N L, Handy N C and Sprik M 2000 *J. Chem. Phys.* **112** 1670
[45] Buttiker M, Imry Y, Landauer R and Pinhas S 1985 *Phys. Rev. B* **31** 6207
[46] Li X X, Wu X J, Li Z Y, Yang J L and Hou J G 2012 *Nanoscale* **4** 5680